Available online at www.sciencedirect.com
SCIENCE DIRECT®
Tectonophysics 370 (2003) 147–162
TECTONOPHYSICS
www.elsevier.com/locate/tecto

Heat transport in serpentinites

U. Seipold*, F.R. Schilling

Divisions 4 and 5, GeoForschungsZentrum Potsdam, Telegrafenberg, D-14473 Potsdam, Germany

Accepted 31 March 2003

Abstract

The thermal transport properties thermal conductivity and thermal diffusivity were examined for a variety of serpentinites as a function of temperature at ambient pressure. The thermal transport properties of serpentinites show an extraordinary behavior. Besides the common $1/T$ decrease in thermal transport properties with increasing temperature, which can be related to an increase in phonon–phonon interactions with increasing temperature, an oscillation of thermal conductivity is observed with maxima around 450 and 850 K. This oscillation is linkable to water release of surficially bounded water and water in pores (450 K) and the dehydration of serpentinite (850 K). The oscillations are explained by advective heat transfer during dehydration, reaching up to 30% of the overall heat transport. The dehydration of serpentinites was examined by XRD and Thermo-Gravimetry and Differential Thermal Analysis/Differential Scanning Calorimeters (TG/DSC) investigations, indicating that the dehydration reaction is kinetically hindered and the crystallization of the product phases are observed at ≈ 1060 K, more than 200 K above the equilibrium of dehydration reactions. The conductive heat transfer by phonons shows a minor temperature variation and dominates thermal diffusivity. Ultrasonic sound velocities as a function of temperature [J. Geophys. Res. 102 (1997) 3051] were used to derive the mean free path length of phonons, which decreases from 0.28 to 0.2 nm at high temperatures. This is in the same order of magnitude as the interatomic distance of O–O, Al–O and Si–O restricting the minimum distance for phononic movement. A high anisotropy in thermal transport properties of single crystallites is concluded from its structure and elastic behaviour. However, the examined samples are macroscopically isotropic. The pressure and temperature dependence of conductive heat transport of an average serpentinite is given by $\lambda=(1/(A+BT))(1+\beta P)$ W/m K, with $A=0.3638$ m K/W, $B=0.000244$ m/W and $\beta=0.148$ GPa^{-1}.

Keywords: Serpentinite; Thermal conductivity; Thermal diffusivity; Advective heat transport

1. Introduction

Temperature gradients are the driving forces that control plate tectonics and the dynamics of metamorphic reactions. The knowledge of thermal parameters is therefore a prerequisite to model the temperature distribution and to understand the ongoing processes within the Earth (e.g. Buntebarth, 1976; Springer, 1999). Nevertheless, thermal transport parameters, such as thermal conductivity or thermal diffusivity, are among the least known petrophysical properties.

Furthermore, the ascent of fluids, the fractionation of elements, and the generation of mantle melts are

* Corresponding author. Tel.: +49-331-288-1875; fax: +49-331-288-1402.
E-mail addresses: seip@gfz-potsdam.de (U. Seipold), fsch@gfz-potsdam.de (F.R. Schilling).

0040-1951/03/$ - see front matter © 2003 Published by Elsevier B.V.
doi:10.1016/S0040-1951(03)00183-5

temperature-controlled by fluid flow and fluid–rock interactions, especially in subduction zone environments. To understand the complex interactions in a dynamic Earth, we need to understand quantitatively the underlying processes and process parameters. The process parameters themselves are interrelated by complex interactions. The heat flow, for example, depends on thermal conductivity of the solid rocks, the advective heat flow by ascending fluids, the internal heat generation by radioactive decay or mineral reactions. The resultant temperature field itself directly influences the heat flow. The advective heat flow through fluids is directly connected to the permeability of the rock and fluid–rock interactions (Balashov and Yardley, 1998). Both, the temperature field and fluid–rock interactions, however, control the permeability of the rock, leading to a complex, probably self-controlling system.

Within the subduction factory, serpentinites play an important role as fluid sink and fluid source during hydration of mantel peridotite to serpentinite and dehydrating of serpentinite to peridotite in the cold part of the mantle (Fig. 1). Within the convecting cell, an increase in pressure and temperature leads to a release of fluids (Kirby et al., 1996).

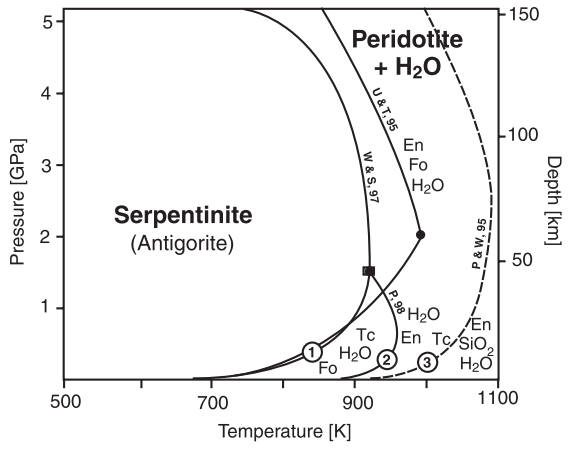

Fig. 1. Simplified phase-diagram for the system peridotite + H_2O. The Phase boundaries are drawn after U & T, 95—Ulmer and Trommsdorff (1995); W & S, 97—Wunder and Schreyer (1997); P, 98—Pawley (1998). ①, serpentinite = talc (Tc) + forsterite (Fo) + H_2O; ②, talc + forsterite = enstatite (En) + H_2O; ③, talc = enstatite + quartz (SiO_2) + H_2O. As we observe no excess talc, the reaction ③ (dashed line) is not realized in our samples.

Serpentinites belong to the ultramafic rocks with the highest water content (about 13 wt.%). As serpentinite seems to be an essential consistent in the subduction process (Peacock, 1993; Giese et al., 1999), the knowledge of its thermal parameters is an important constraint in understanding subduction processes, such as intermediate depth earthquakes (e.g. Schilling et al., 2000; Peacock, 2001), or fluid-ascent and fluid-driven melting of hot mantle peridotite (e.g., Davies, 1999).

The thermal transport properties thermal conductivity λ and thermal diffusivity a of rocks show usually a decrease with increasing temperature, which can be described by a $1/(A+BT)$ dependency (Seipold, 1998). This $1/T$ dependency is typical for a phononic heat transfer (Eucken, 1911) and the result of an increase in phonon–phonon interactions leading to a decrease in the mean free path length of phonons, l, with rising temperature. Thermal diffusivity and mean free path length of phonons are related by the mean phonon (acoustic) velocity v (e.g. Kittel, 1983) according to

$$a = \frac{1}{3} vl \tag{1}$$

At high temperatures an increase in thermal conductivity and thermal diffusivity is reported for some rocks (e.g. suevite, Schilling, 1999) and minerals (e.g. orthoclase, Hoefer and Schilling, 2002), due to a radiative heat transport component. The radiative heat transfer is characterized by a T^3 dependency for homogeneous samples of infinite length, if the extinction coefficient does not depend on temperature. For one sample, an increase in thermal diffusivity was described during ongoing dehydration (Schilling, 1997).

The thermal transport properties of serpentinised ultrabasite have been studied previously by Petrunin and Popov (1981, 1994) up to 700 K, well beneath the temperature, where the major dehydration takes place. They showed that even a minor amount of serpentinite suffices to change thermal transport properties of altered lherzolites and harzburgites significantly. The pressure dependence of thermal conductivity and thermal diffusivity has been presented and discussed by Seipold (1996) for a collection of serpentinites up to 500 MPa.

Table 1
Sample description

Location	Sample	Sample description, mineral content (%)	Density [g/cm^3]
Saxonian Granulite Massif			
Reinsdorf	GR85-5	lizardite (97), pyroxene (1), accessory (2)	2.63
	GR85-7-1, 2, 3 Reinsd 1+2	lizardite (73), pyroxene (24), accessory (3)	2.73
	GR85-8-1 Reinsd 3+4	lizardite (96), chromite (2), accessory (2)	2.49
Nossen	GR35-37	lizardite (97), chromite (1), accessory (2)	2.53
	GR85-40	lizardite (93), pyroxene (3) chromite (1), accessory (3)	2.58
	GR85-36	lizardite (94), pyroxene (3) chromite (1), accessory (3)	2.57
Bohrberg	GR85-49+ 49-2	garnet bearing serpentinite	>2.7
Gilsberg	GR85-115/2	garnet bearing serpentinite	>2.7
Waldheim	Waldh1	porosity 0.36%	2.74
Hohenstein–Ernstthal	ScheibenbA	hydrated basalt, porosity 0.47%	2.96
Crete Island			
	Kreta 1+2	serpentine minerals (98) mainly chrysotile (>80), minor lizardites, magnetite (2), SiO_2 (27.16 mol%), MgO (39.86 mol%), FeO_{tot}. (0.84 mol%), H_2O (29.51 mol%) porosity 4%	2.66
Saxonian Erzgebirge			
Niederlochmühle	E85-55	garnet bearing serpentinite	>2.7
Oberlochmühle	E85-57	garnet bearing serpentinite	>2.7

We have chosen natural serpentinites of different origin to study different thermal transport processes especially during dehydration. The goal of this contribution is to understand some of the complex interrelations of thermal transport properties of serpentinites and to narrow the range of possible process parameters within the subduction factory.

This contribution is substantially enriched and motivated by H. Kern, by stimulating discussions and his fundamental work to the petrophysical properties of rocks, especially his contribution about elastic properties of serpentinites. His measurements of the elastic properties of serpentinites (Kern et al., 1997) are the basis of the structural interpretations of the presented results.

1.1. Investigated samples

The thermal transport properties of massive serpentinised ultrabasites were studied, representing well-characterized and typical assemblages (Table 1). The majority of samples investigated were taken from freshly broken compact rocks found in quarries of the Saxonian–Granulite Mountains (SE Gemany). The dimensions of these serpentinite bodies range from meters to kilometers. They are often embedded in concordantly as lenses in a granulite matrix. The serpentinites were formed by serpentinisation of ultrabasic rocks. After Kopp (1986) and Werner (1987), most of the mother rocks belong to a lherzolitic series of alpinotype peridotites, with ≈ 50 vol.% olivine and ≈ 40 vol.% clinopyroxene. Relics of the product minerals were found in the centers of serpentinite meshes. The serpentinites are fine-grained and dense rocks. Microscopic investigations show that the grains

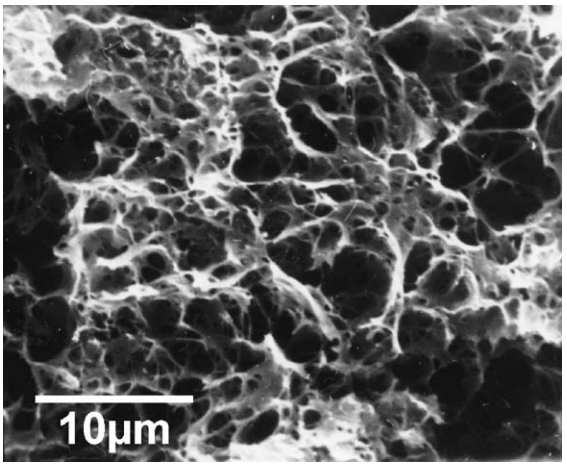

Fig. 2. Typical mesh-structure of examined serpentinites. (Diethensdorf; Kopp, 1986).

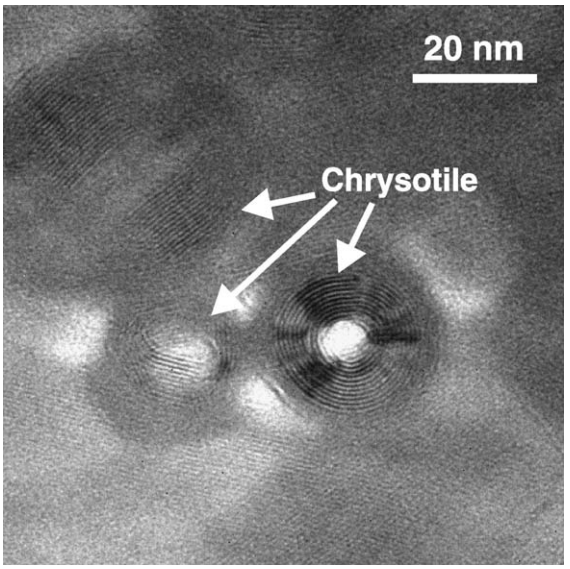

Fig. 3. Transmission electron microscopic image of serpentinite from Crete. Oriented section of the sample shows that main serpentine modification is chrysotile, which is embedded in a lizarditic matrix. Arrows mark chrysotile-crystals with different orientations.

are build-up as typical serpentine meshes (Fig. 2). The diameter of the meshes is of the order of a few micrometers. The investigated samples showed a pseudomorphic fabric. The grain boundaries of the original peridotites are marked by magnetite exsolutions. Most serpentinite bodies show a periodic layering, which is explained by magmatic differentiation of the former peridotite (Kopp, 1986; Werner, 1987). The thickness of the layers differs from some centimeters to 1 m. Furthermore, some very similar serpentinites from the Saxonian Erzgebirge (Germany) and a few samples from Crete (Greece) were investigated for comparison.

X-ray diffraction analysis in combination with TEM studies revealed that lizardite is the dominating serpentine mineral in the majority of the investigated samples. The black color of the serpentinite samples is a consequence of very fine-grained magnetite crystals dispersed in the lizardite. Microscopically, a conjugated system of small cracks filled with magnetite is observed in some samples. During the experiments, magnetite oxidized to hematite at high temperatures. Thus, during the experiments, the originally black or dark gray samples changed to red. Chemical analysis of similar samples from the Granulite Massif showed a magnetite content in the order of 5% (Kopp, 1986). The serpentinite sample from Crete mainly consists of chrysotile in a lizardite matrix (Fig. 3). A small amount of magnetite (< 5%) is revealed by Rietveld

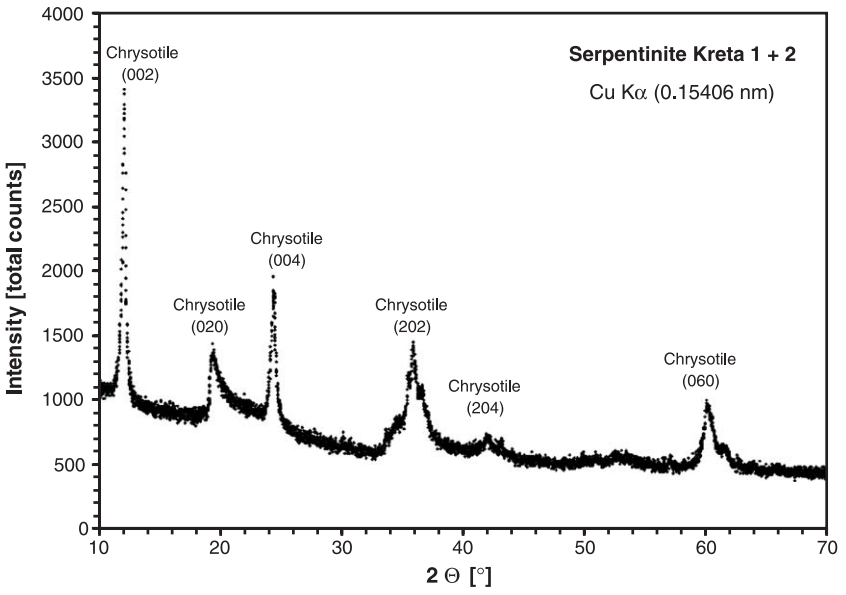

Fig. 4. X-ray diffraction (XRD)-pattern of sample Kreta 1 + 2. Besides serpentine minerals, only a minor magnetite content is revealed by Rietfeld-refinement (GSAS) of the spectrum.

refinement of X-ray diffraction spectra on powdered samples (Fig. 4).

2. Experimental

Thermal conductivity and thermal diffusivity of the serpentinite samples were determined simultaneously using a specially designed transient method in a cylindrical geometry. Experiments were performed at various temperatures at ambient pressure. To reduce the influence of thermal cracking during the experiments, temperature was increased slowly. For a detailed discussion, see Seipold (2001). A heat pulse is generated by a line source in the center axis of the cylindrical rock sample. The heat pulse has a finite length of 3 s. The resultant thermal pulse leads to a temperature equilibration process and propagates in radial directions. At about half the distance between line-source and surface of the rock cylinder, a thermocouple registers the arriving thermal pulse. The thermal diffusivity is deduced from the travel time of the pulse and the distance between heater and thermocouple. For the determination of thermal conductivity, the height of the arriving peak, the released energy from the heating pulse and the thermal diffusivity are used. For details of the evaluation procedure, see Seipold (1988).

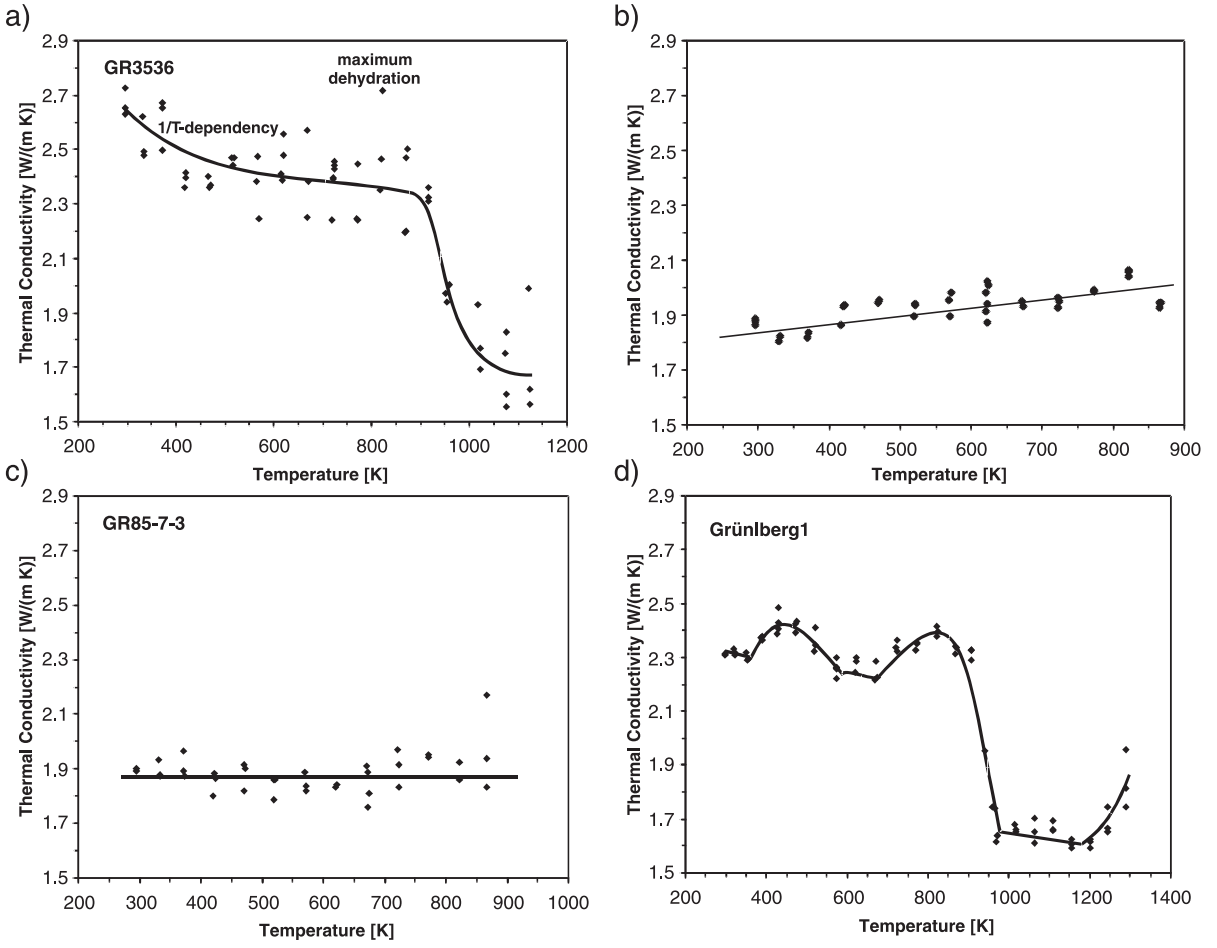

Fig. 5. Thermal conductivity of different serpentinite samples. Thermal conductivity of serpentinites from different origins varies significantly. Most samples show an oscillation of thermal conductivity (a, d). Other samples show a small to negligible temperature dependence of thermal conductivity (c) or even an unusual linear increase with increasing temperature (b).

Table 2
Conductive heat transfer of serpentinites. Samples with a small portion of advective heat transfer

Sample	*A* [(m K)/W]	*B* [(m K)/W/K]*10 000
GR85-5	0.400	2.8
GR85-40	0.215	6.1
GR85-49-2	0.325	4.8
GR85-49	0.465	1.1
GR85-36	0.298	2.7
Reinsd4	0.405	2.4
GR85-115	0.387	2.2
GR85-155-2	0.441	0.6
Waldh1	0.209	7.8
E85-55	0.304	0.5
Average	0.364	2.44

The observed thermal conductivity λ is approximated according to $\lambda=((1)/(A+BT))$.

The rock samples were 43 mm in length and 27 mm in diameter. The measurements were carried out from room temperature up to 1300 K, every 50 K. At each temperature step, ≈ 30 min was necessary to approach thermal equilibrium. The mean of three measurements was used at each temperature step. To avoid an overlapping of the heat pulse signals, a delay time between the measurements of at least 5 min was allowed. For the measurements under dehydration or other transient conditions, a short duration of the experiments is essential. The advantage of the applied method is the short measuring time of 40 s. Therefore, the experimental conditions did not change much during the short time intervals. The precision of the apparatus is better than 3% for thermal diffusivity and 5% for thermal conductivity experiments for all examined samples. During the dynamic processes of dehydration and crystallization the measured thermal diffusivity may vary more than the precision of the apparatus. This is a consequence of the short time that is required to dehydrate and crystallize the sample. Therefore, thermal diffusivity varies due to dynamic changes within the sample at one temperature.

The loss on ignition, L.O.I., and change in heat capacity were determined simultaneously with combined Thermo-Gravimetry and Differential Thermal Analysis/Differential Scanning Calorimeters (TG/DSC), using ≈ 40 mg of fine-grained powder. The LOI and heat capacity were studied with a scanning rate of 10 K/min. To avoid the influence of predrying of the samples in commercial TG/DSC devices, further L.O.I. determinations were carried out on fresh powdered samples, with temperature steps of 25 K. The samples were held at each temperature for 5 and 30 min, respectively. After each temperature step, the mass change was recorded by a high precision balance (Sartorius).

The samples were characterized using high-resolution X-ray diffraction studies. The shapes of crystallites were characterized by TEM studies (Philips). The chemical composition of the whole rock was

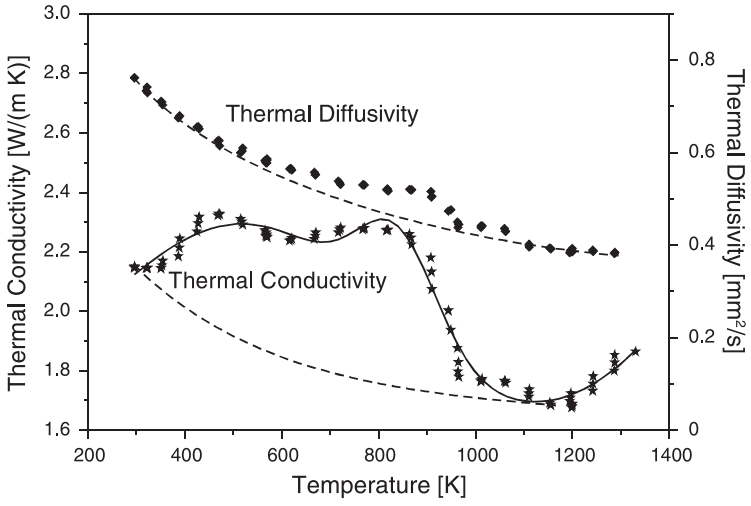

Fig. 6. Thermal conductivity and thermal diffusivity of a serpentinite sample from Oberlochmühle (E85-57).

determined by X-ray fluorescence analysis on glass pellets (Siemens).

3. Results

The scattering of the measurement data points, especially at higher temperatures, is much greater than the precision of the apparatus, indicating dynamic variation of the sample, e.g. due to dehydration and crystallization, which leads to a scattering of sample properties. Due to reactions with the filament, the line source was often destroyed at temperatures well beneath 1300 K (Fig. 5). To reduce the scatter of the thermal conductivity data, Fourier-based filters were used.

During the systematic study of thermal transport properties of different rock types (Seipold, 1988, 1990, 1992, 1995, 1996, 1998, 2002; Seipold and Huenges, 1998; Seipold et al., 1998; Schilling, 1997, 1999; Arndt et al., 1997; Hoefer and Schilling, 2002; Tommasi et al., 2001), serpentinites exposed the most extraordinary behavior of all investigated rocks. As described, thermal diffusivity and thermal conductivity of common rocks decrease with increasing temperature for lower and intermediate temperatures. Only for some rocks a significant radiative heat transfer component becomes apparent at temperatures exceeding 800 K. Despite serpentinite samples that show the classical $1/T$ behaviour of thermal conductivity and thermal diffusivity (Fig. 5a, Table 2), for some samples an increase in the thermal transport parameters with increasing temperature is observed (Fig. 5b), and some samples have a nearly negligible temperature dependence of thermal conductivity (Fig. 5c).

Table 3
Conductive and advective heat transfer of serpentinites

Sample	A (m K/W)	B [(m K/W/K)*10 000]	C (W/m K)	D (W/m K)	s (K)	s_2 (K)	w (K)	w_2 (K)
GR85-5	0.400	2.80	0.358	0.105	781	485	106	131
GR85-7-1	0.224	1.35	1.264	0.628	806	456	199	60
GR85-7-2	0.490	0.90	0.185	0.07	808	550	94	100
GR85-7-3	0.495	1.00	0.198	0.021	829	476	127	88
Reinsd1	0.426	5.80	0.867	0.394	901	515	210	167
Reinsd2	0.605	0.00	0.396	0.227	946	415	226	181
GR85-37	0.785	0.00	1.264	0.1	894	418	210	84
GR85-40	0.209	6.30	1.01	0.646	807	513	103	129
GR85-49-2	0.323	4.80	0.559	0.363	851	586	106	134
GR85-49	0.465	1.05	0.326	0.393	813	372	199	78
GR85-36	0.298	2.70	0.364	0.333	880	708	67	131
GR85-8-1	0.738	0.00	0.528	0.404	739	482	96	60
Reinsd3	0.211	12.6	0.958	1	903	600	126	228
Reinsd4	0.405	2.42	0.494	0.286	831	600	65	110
GR85-115	0.387	2.21	0.297	0.214	825	620	69	140
GR85-115-2	0.441	0.55	0.33	0.405	794	521	76	212
Waldh1	0.209	7.78	0.544	0.788	884	688	49	212
ScheibenbA	0.530	0.00	0.16	0.113	850	503	204	68
Grünlberg1	0.630	0.20	0.526	0.822	830	450	100	265
Grünlberg2	0.647	0.02	0.405	0.74	831	393	78	300
KretaP1	0.486	1.07	0.396	0.462	857	567	75	225
KretaP2	0.466	1.21	0.309	0.38	866	645	60	212
E85-55	0.340	0.54	0.117	0.103	850	459	93	43
E85-57	0.498	0.81	0.422	0.449	828	522	90	180
Average	0.446	2.34	0.512	0.394	842	522	118	147

The measured thermal conductivity λ is approximated according to

$$\lambda = \frac{1}{A + BT} + C \exp\left(-0.5\left(\frac{T - s_1}{w_1}\right)^2\right) + D \exp\left(-0.5\left(\frac{T - s_2}{w_2}\right)^2\right).$$

In addition to these different temperature dependencies of thermal transport parameters, an overlaying oscillation of thermal conductivity λ is observed for most samples (Fig. 5d). The whole temperature dependence of the observed thermal conductivity can be well approximated (Fig. 6), if two Gaussian functions are added to the classical conductivity equation:

$$\lambda = \frac{1}{A + BT} + C \exp\left(-0.5\left(\frac{T - s_1}{w_1}\right)^2\right) + D \exp\left(-0.5\left(\frac{T - s_2}{w_2}\right)^2\right) \quad (2)$$

with A and B as the "classical" parameters for thermal conductivity (Seipold, 1998), C and D representing the amplitude of the oscillation, s_1 and s_2 the position of maxima in thermal conductivity, and w_1 and w_2 the width at half maximum of the Gaussian curve. The observed behavior was approximated by a least-square algorithm to Eq. (2), systematically minimizing the quadratic deviation between measured and modeled curve. The as-derived thermal parameters are listed in Table 3.

The first maximum changes in position (s_1) and width (w_1) a lot, but the second maximum always appeared around 842 ± 35 K (s_2) with a smaller variability in width (w_2) (Table 3). Surprisingly, a smaller oscillation is observed for thermal diffusivity of the samples (Fig. 6, Table 3). At higher temperatures, above 800 K a shallow maximum superposes the temperature dependence of thermal diffusivity (Fig. 6).

To quantify the temperature dependence of dehydration, TG/DTA experiments were carried out. The TG/DTA results in Fig. 8 on a predried sample (at 450 K for more than 24 h) in a vacuum chamber show that most of the water release of about 13 wt.% is concentrated in a narrow temperature range. Two overlapping endothermic reactions are observed in the DSC signal during dehydration (Fig. 7). Furthermore, the kinetics of dehydration was studied by TG measurements at different heating rates (5 and 30 min/temperature step) on fresh samples without vacuum. The release of free water and water absorbed at surfaces is clearly resolved at temperatures around 400 K (Fig. 8). If the same temperature program is chosen as for the measurements (30 min/temperature step) of thermal transport properties, a strong mass release (TG) is observed around 900 K, which is in the

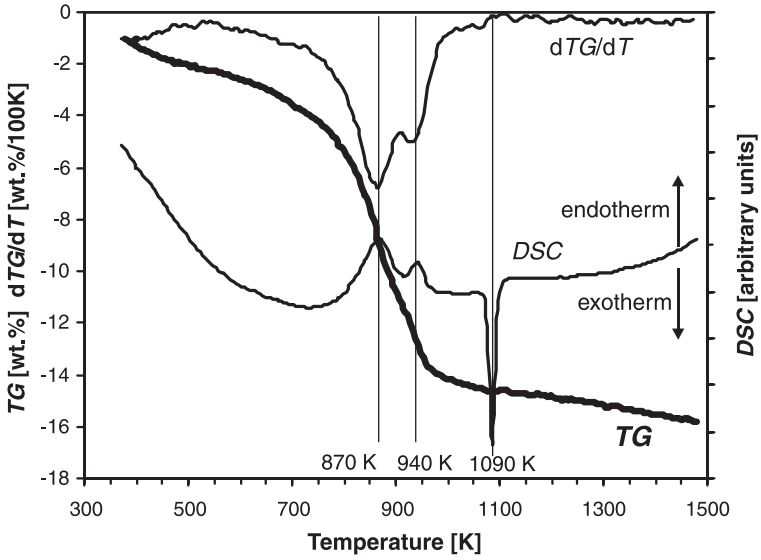

Fig. 7. Result of a simultaneous TG/DSC experiment. A stepwise dehydration is observed with a maximum at 870 and 940 K (minimum in dTG/dT and maximum in DSC – endothermic reaction enthalpy).

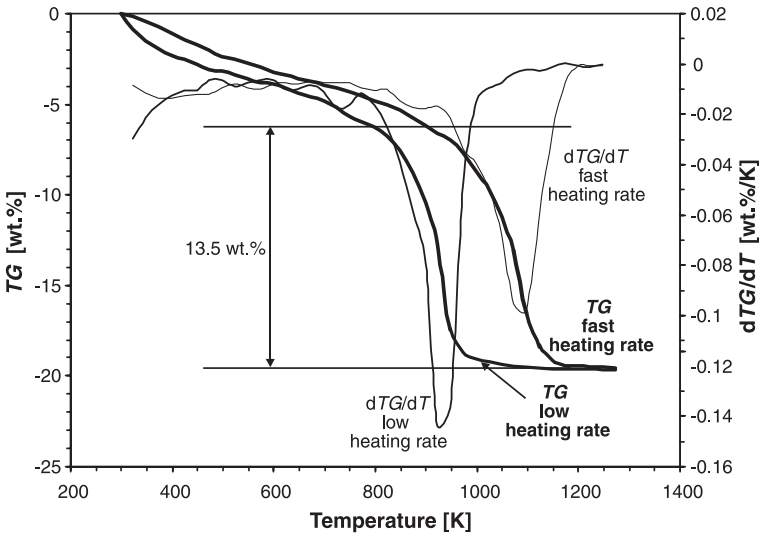

Fig. 8. *TG* experiments to determine the temperature dependence of L.O.I. at different heating rates. Fast heating rate corresponds to more then 20 K/min, low heating rate is ≈ 1 K/min.

same range as the maximum of oscillation of thermal conductivity (Fig. 6).

4. Discussion

4.1. Advective heat transfer

The main focus of this contribution is to discuss the unusual thermal transport properties of serpentinite, showing a strong oscillation in thermal conductivity and a minor oscillation in thermal diffusivity λ. For conductive heat transfer in a homogeneous body, thermal diffusivity a and thermal conductivity are interrelated by the heat capacity C_P and the density ρ according to

$$\lambda = c_P \rho a. \quad (3)$$

If the observed oscillation would be due to conductive heat transfer (Eq. (3)) should hold true and the variation of λ would be the result of variations in heat capacity and/or density. The known variation in heat capacity is much smaller than the observed variations in thermal conductivity. The dehydration reactions lead to a decrease in density during dehydration. Consequently, the variations in heat capacity and density would lead to a minor decrease in thermal conductivity, with respect to thermal diffusivity; however, the opposite is observed. Therefore, the observed increase in thermal conductivity during dehydration cannot be explained by variations of heat capacity and density.

In other words, the assumption of a pure conductive heat transfer leads to a discrepancy to experimental observations, and another heat flow mechanism has to be taken into account. Therefore, we propose a superposition of two heat transfer mechanisms. One part of the heat is transported by heat conduction, whereas another part of the heat is carried advectively by steam, leaving the sample after the dehydration process. If we would consider a storage of the freed fluid in the small pore space of the sample (<4 vol.%) already a small temperature increase would lead to a additional pore pressure of some 100 MPa. This overpressure results from the dehydrating serpentinite leading to an volume increase. In addition to that, the high thermal expansion of the fluid compared to the expansivities of minerals will lead to an overpressure, if the fluids are trapped in pores. The overpressure exceeds the tensile strength of the host rock, leading to small cracks or the observed failure of some samples. The cracks are capable to effectively transport heat through an advective process away from the heating wire. The resultant Dracy flow of the fluid

will carry heat away from the heating wire to the outer surface of the sample.

In the DSC signal (Fig. 7) an endothermic latent reaction enthalpy is observed. This latent heat might consume some of the energy during the activity of the filament. This would result in a lower travel time of the heat pulse to the thermocouple and therefore to a signal, which would be interpreted as a lower thermal diffusivity. From the DSC experiments (Fig. 7) we know that an endothermic latent heat had to be taken into account, and a reduction in thermal diffusivity should result. However, a small increase in thermal diffusivity is registered (Fig. 6). Both latent heat as well as variations in heat capacity and density seems not to be responsible for the observed oscillations in thermal conductivity. As a consequence, the fundamental change in heat transport capability above the dehydration reaction may be the result of a third heat transport mechanism, e.g. radiative heat transfer, or of a major change in the heat transport process.

As clearly resolved in TG (Figs. 7 and 8) and DSC (Fig. 7) measurements, a strong dehydration takes place around 900 K leading to a weight loss of ca. 13.5 wt.%. At 0.1 MPa, serpentinite $Mg_6Si_4O_{10}(OH)_8$ dehydrates to forsterite (Mg_2SiO_4) and talc ($Mg_3Si_4O_{10}(OH)_2$. The dehydration of talc and the reaction with forsterite leads to enstatite ($MgSiO_3$).

$$5\ Mg_6Si_4O_{10}(OH)_8 = 12\ Mg_2SiO_4 + 2\ Mg_3Si_4O_{10}(OH)_2 + 18\ H_2O$$

$$Mg_2SiO_4 + Mg_3Si_4O_{10}(OH)_2 = 5\ MgSiO_3 + H_2O$$

The two steps of the dehydration reactions are clearly resolved in the DSC signal (Fig. 7). In the TG experiments, both dehydration reactions overlap and are visible as a change in the dehydration curve (Fig. 7). The dehydration reaction and crystallization of the products are kinetically hindered (Faust and Fahey, 1962) and an amorphous material is observed in the temperature range between dehydration and crystallization of enstatite and forsterite. Therefore, the exothermic reaction from dehydrated talc and serpentinite to forsterite and enstatite takes place at higher temperatures (peak around 1090 K). Additional XRD measurements strongly support this interpretation, as they reveal only enstatite and olivine as products for samples after the thermal conductivity experiments. No quartz (qtz) was observed in XRD measurements, which would appear for samples with excess in talc.

The crystallization of enstatite and forsterite should increase thermal conductivity and thermal diffusivity significantly because at 1000 K both minerals have much higher thermal conductivity values of ≈ 3 W/m K (Tommasi et al., 2001) compared to that of serpentinite reaching ≈ 1.5 W/m K (this study). For the few samples were it was possible to measure thermal conductivity and thermal diffusivity above 1060 K, which correspond to the temperature of enstatite and olivine crystallization, a pronounced increase in thermal conductivity is observed (Figs. 5d and 9).

At lower temperatures (<450 K) a minor L.O.I. is observed, which is related to the desorption of water at grain surfaces and the release of water out of pores, which is less than 2 wt.% as the porosity is smaller than 4 vol.%. Between 450 and 900 K a continuous L.O.I. is observed and attributed to a small but steady dehydration of structurally bonded water in serpentinite. Petrological experiments and structural refinements from XRD studies by Wunder et al. (2001) indicate a continuous dehydration of serpentinite, leading to an increase in the OH-dependent lattice spacing. If water release is responsible for the observed oscillation in thermal conductivity, one should expect two maxima in thermal conductivity, one around 450 K from desorbed water and water release from pores, and another one around 900 K. This is in concordance to the observations (Figs. 5d, 6 and 9).

The apparatus to measure thermal conductivity and thermal diffusivity is designed for conductive heat flow. Thermal diffusivity describes an equilibration or diffusion process and is therefore characterized by the travel time of the heat pulse from the filament to the thermocouple. However, the observed oscillation in thermal conductivity has a negligible effect on thermal diffusivity.

The deduced thermal conductivity is a measure of the amount of the transferred heat. The strong oscillation in thermal conductivity is therefore a direct measure of the portion of advective heat transport to the overall thermal conductivity. An additional support for our advective heat transport model for ser-

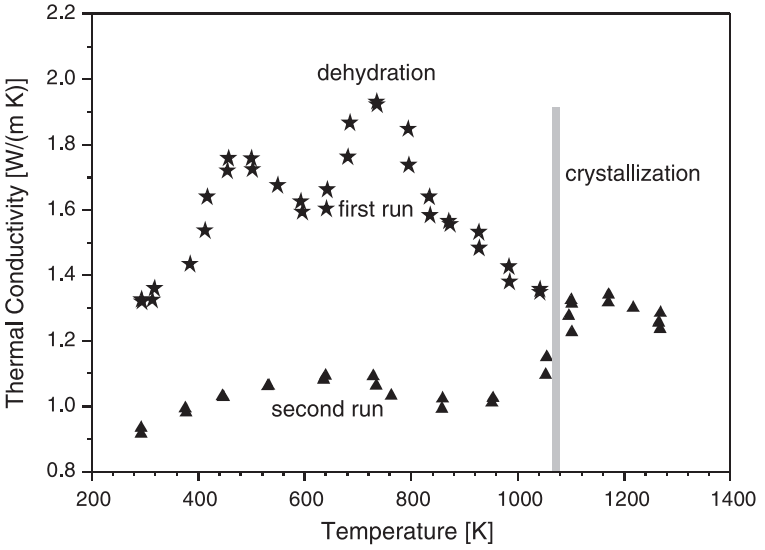

Fig. 9. Thermal conductivity of serpentinite as a function of temperature. A serpentinite sample was measured during a first run to a maximum temperature (1050 K) well above the dehydration reaction (Fig. 4), but below the exothermic crystallization at 1090 K (Fig. 4). Then, the sample was cooled down to room temperature and the experiment was repeated to 1300 K, a temperature well above the crystallization temperature.

pentinites results from the observation (Fig. 10) that the temperature dependence of thermal conductivity follows the dehydration rate (d*TG*/d*T*).

That dehydration is the reason for oscillation in thermal conductivity is further strengthened by a specially designed experiment. A serpentinite sample was measured during a first run (Fig. 9) to a maximum temperature (1050 K) well above the dehydration reaction (Fig. 7), but below the exothermic crystallization at 1090 K (Fig. 7). Then, the sample was

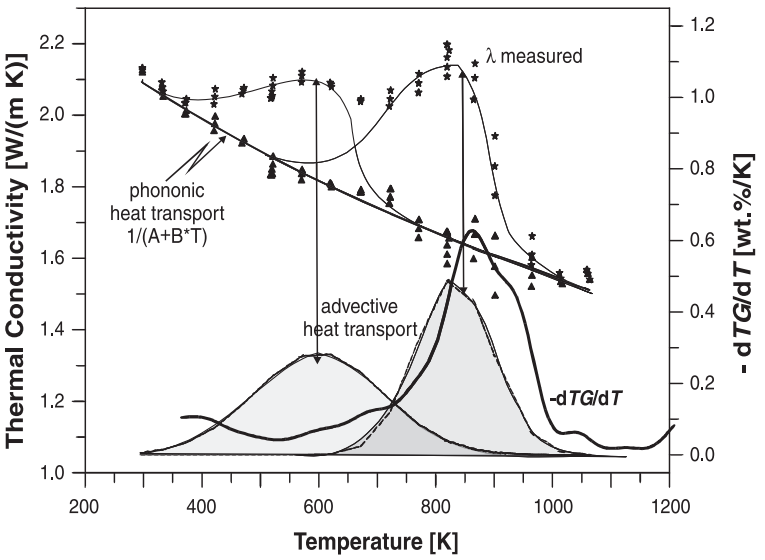

Fig. 10. Thermal conductivity of serpentinite as a function of temperature compared to *TG* measurements. The maximum of the oscillation in thermal conductivity corresponds to the maximum in − d*TG*/d*T*. The grey shaded areas are related to the advective portion of heat transfer.

cooled down to room temperature and the experiment was repeated to 1300 K, a temperature well above the crystallization temperature. In the first run the typical two maxima are observed (Fig. 9, first run). Both maxima are completely missing in the second run (Fig. 9, second run) because all water is removed during the first run. The absolute value of thermal conductivity during the first run is much higher than during the second run. The dehydration and cooling of the sample lead to the creation of micro-cracks, which causes a decrease in thermal conductivity. The amorphous phase resulting during the dehydration process (Faust and Fahey, 1962) will further reduce thermal conductivity. At higher temperatures, the cooling-induced micro-cracks will disappear by thermal expansion and, consequently, thermal conductivity will increase. Furthermore, during the crystallization process forsterite and enstatite appear, which both have a high thermal conductivity. As a consequence, the thermal conductivity increases during the crystallization at 1090 K. The curvature observed for the second run (Fig. 9) cannot be explained by a radiative heat transport mechanism, which would result in a T^3 dependency and not in the observed sharp change in thermal conductivity at 1090 K. Therefore, we conclude that the observed behavior is the result of crystallization and closure of thermally induced micro-cracks.

The advective portion of thermal conductivity is deduced by subtracting the conductive heat transport ($1/(A+BT)$, Eq. (2)) from the measured conductivity (Fig. 10). The average advective portion of thermal conductivity and standard deviation is shown in Fig. 11. The advective heat flow is responsible for more than 30% of the overall thermal conductivity during dehydration.

The amount of free water responsible for advective heat flow seems to be very small, as the experiments were performed in an open system, allowing the freed fluid to be released immediately. This is supported by the observation that the oscillations of thermal transport properties coincide with the dehydration of serpentinite within the experimental uncertainties (Figs. 5d, 5d, 7, 8, 9 and 10). If the fluid could remain for a long period, the maximum of the oscillation in thermal conductivity (Figs. 5d and 10) would appear at higher temperatures than the minimum in dTG/dT (Figs. 7 and 8).

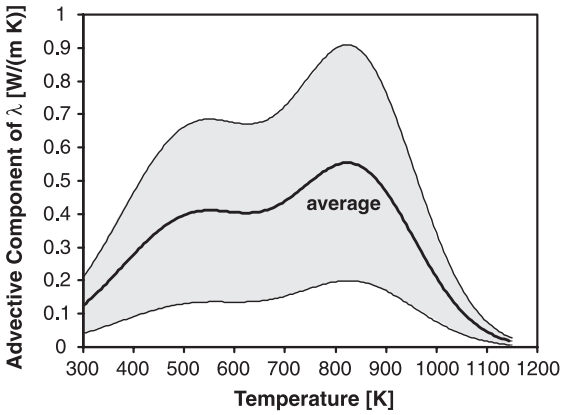

Fig. 11. Advective component of thermal conductivity λ as a function of temperature. The grey shaded area represents the 1σ deviation of the average advective heat transfer.

The advective heat flow depends on the amount of fluid (pore space) and permeability of the rock (Raab, personal communication) and the transport capability of the fluid. Samples with a small oscillation in thermal conductivity (Fig. 5b and d) point to a pore space that leads to a sudden loss of freed fluid and, therefore, negligible heat transfer by advection. The low porosity (< 2 vol.%) and permeability but a high advective heat transport of most of the examined metamorphic rocks shows that the transport capability of fluids is very high. As the experiments were performed under non-steady-state conditions, the amount of released fluid varies between two experiments, even at the same temperature. However, this variation is small compared to the observed oscillation. As the amount of released fluids at each temperature step is much less than 1%, the measured advective heat transfer corresponds to rock with a low portion of fluids ($\approx$ 0.1 vol.%) in an interconnected pore space. In nature, the amount of free fluid may be even higher, however, one would expect that, on the other hand, the interconnected pore space should be lower. Therefore, the experimental results prove a significant advective heat flow in serpentinites, which can be in the same order of magnitude as or even exceeds heat transfer by phonons.

The observed high advective heat transfer is in good agreement with finite difference calculations and thermal diffusivity experiments by Schilling (1997), showing that only a very small amount of fluids

suffices to enhance thermal transport properties significantly. This is mainly due to the high fluidity and heat capacity of H_2O, which results in a high heat transport capacity of this fluid.

4.2. Conductive heat transfer

Despite the important advective heat transport component, conductive heat transfer dominates thermal transport properties and its temperature dependency, mainly by a phonon mechanism. The phononic heat transport is deduced from thermal diffusivity measurements, where only a very minor advective heat transfer component is observed. In addition to that, the A and B parameters of samples with a low advective heat transfer component (Fig. 5b and c) were used to determine phononic heat transfer (Table 2). The determined average phononic thermal conductivity is plotted in Fig. 12. The gray shaded area represents the 1σ range of the average conductivity. The phononic portion of thermal conductivity (Fig. 12) is approximated by the typical $1/(A+BT)$ dependency, which is related to an increase in phonon–phonon interactions with increasing temperature (Eucken, 1911). The average thermal conductivity slightly decreases from 2.4 W/m K at ambient conditions to 1.6 W/m K at 1200 K. The observed temperature dependence is much lower than the temperature dependence of peridotites of comparable composition (Tommasi et al., 2001) or oxides (e.g. MgO, Clauser and Huenges, 1995; quartzite, Schilling, 1999), where thermal conductivity decreases by more than 80%.

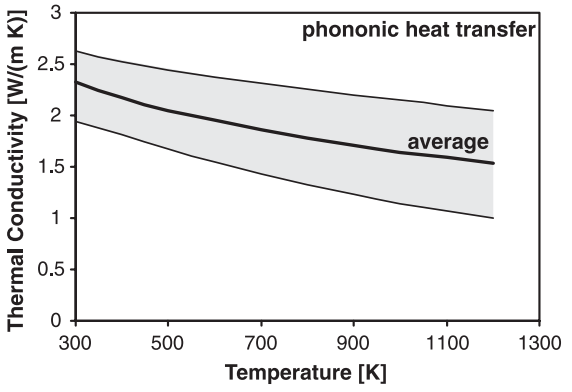

Fig. 12. Conductive thermal conductivity λ as a function of temperature. The grey shaded area represents the 1σ deviation of the average conductive heat transfer.

The differences in the temperature dependence of thermal diffusivity of serpentinites, peridotite and oxides may be the result of different temperature dependences of phononic velocity v and/or mean free path length l (Eq. (1)). As sound velocity of serpentinites only decreases by a few percent per 100 K (e.g. Kern et al., 1997), the observed temperature dependence of thermal conductivity (Fig. 12) is mainly caused by variations in the mean free path length of phonons.

To quantify the variation in mean free path length of phonons, the average sound velocity of serpentinites needs to be known by an independent experiment. By chance, there is a detailed study on acoustic velocities of a collection of serpentinites, providing the temperature dependency of sound velocities of serpentinite (Kern et al., 1997). The mean free path length of phonons is deduced according to Eq. (1), using the average sound velocity

$$v = \sqrt{\frac{v_P^2 + v_{S,1}^2 + v_{S,2}^2}{3}} \tag{4}$$

as average velocity of phonons v (Fig. 13). A consequence of the model use is that only the conductive portion of thermal diffusivity has to be applied in Eq. (1) to deduce the mean free-path length of phonons using the average sound velocity (Eq. (4)), without the advective portion of heat transfer. The average phononic velocity decreases from $\approx$ 5.02 km/s at ambient conditions to 4.85 km/s at 900 K. In the same temperature interval, the mean free path length of phonons decreases from 0.28 to 0.21 nm. At higher temperatures the mean free path length of phonons tends to 0.2 nm. This is in the same order of magnitude as the interatomic distance of O–O (0.28 nm), Al–O (0.19 nm) and Si–O (0.181 nm) using the data by Shannon (1976). The interatomic distances restrict the minimum distance for phononic movement and therefore the validity of the classic phonon model. Hence, if the mean free path length of phonons is in the range of interatomic distances, no further reduction in mean free path length can be expected through further phonon scattering (e.g. Berman, 1984) and the classical $1/(A+BT)$ is no longer valid. As at ambient conditions the mean free path length of phonon for

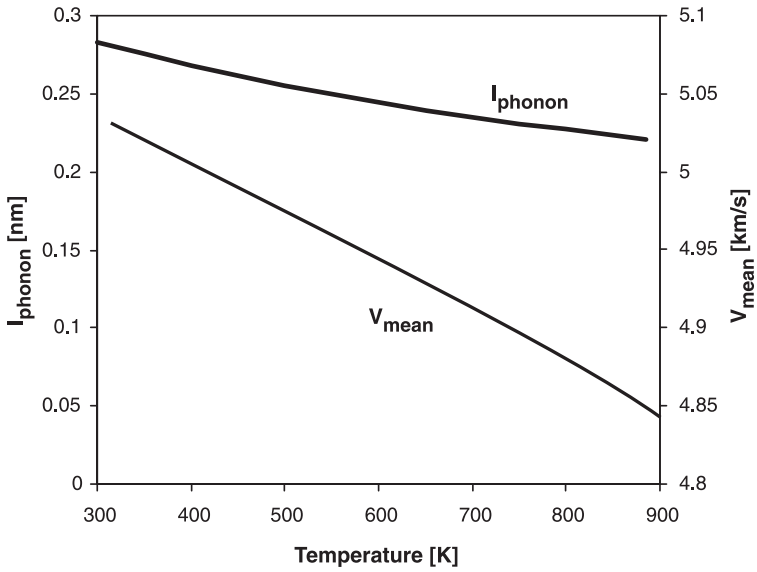

Fig. 13. Average mean free path length of phonons as a function of temperature, determined by Eq. (1) using the mean sound velocity $v = \sqrt{(v_P^2 + v_{S,1}^2 + v_{S,2}^2)/(3)}$. The sound velocities and their temperature derivatives were taken from Kern et al. (1997).

serpentinites is already in the range of interatomic distances, only a small reduction in the mean free path length is possible.

This high scattering of phonons at lower temperatures is the result of phonon–phonon scattering and scattering at lattice imperfections including grain boundaries and chemical inhomogeneities. The high number of atoms in the unit cell leads to a high number of phonon states and, hence, high phonon scattering even at room temperature (Slack, 1973). In addition, phonons will be scattered by impurities and defects (point defects, dislocations and 2D defects such as grain boundaries, boundaries between submicroscopic crystals in the serpentinite meshes). Further scattering due to the mass differences of ions (Fe, Mg, Si, Al, O) and different binding strengths (Schilling, 1998) should further reduce the mean free path length in serpentinite. In other words, the described complexity of the serpentinite structure already reduces the mean free path length at room temperature significantly. Therefore, serpentinites show small temperature dependence in thermal conductivity, but oxides or peridotites, which have a higher mean free path length at ambient conditions, show a much stronger temperature dependence of mean free path length.

Serpentinites show a high anisotropy in sound velocity measurements (Kern et al., 1997). This is mainly caused by the strong difference in binding strength parallel and perpendicular to the cleavage, similarly to micas. According to Eq. (1), the high anisotropy in sound velocity will lead to a high anisotropy in thermal transport properties of single crystallites. In analogy to micas, the mean free path length of phonons perpendicular to the cleavage should be much smaller than the mean free path length parallel to the cleavage, leading to an additional contribution to anisotropy of serpentinites, despite the differences in sound velocities (Eq. (1)). Sound velocity experiments (Kern et al., 1997) and structural similarities strongly point to a high anisotropy in thermal transport properties of serpentine crystals. However, in our macroscopic samples, this anisotropy is effectively eliminated by the nearly statistic distribution of the orientations of the crystal.

4.3. Pressure dependence of thermal conductivity

The pressure dependences of thermal conductivity and thermal diffusivity of some of the investigated serpentinites were examined previously by Seipold (1996) up to 500 MPa simultaneously. The derived

mean pressure coefficients were $\alpha = 14.8 \pm 6.0\%$/GPa and $\beta = 13.4 \pm 7.4\%$/GPa for thermal conductivity and thermal diffusivity, respectively.

According to Eq. (1), the intrinsic pressure dependence of thermal diffusivity—which is a consequence of the variation in thermal transport properties of minerals—is related to the variation in the phononic velocity and mean free path length of phonons. The variation of the velocity of phonons is well known by ultrasonic studies conducted by Kern et al. (1997) as a function of pressure. The observed pressure dependence in mean sound velocity reaches $3.4 \pm 0.5\%$/GPa. The pressure dependence of sound velocity of some of the samples investigated for thermal transport properties was determined by Raab (personal communication) showing a slightly higher pressure dependence around 5%/GPa. Both ultrasonic studies reveal a three times lower pressure dependence for sound waves than for thermal transport properties. The observed deviation in pressure derivatives of sound waves and thermal transport properties cannot be explained by variations in the mean free path length within the crystals alone. Therefore, additional scattering mechanisms, e.g. at grain boundaries within the mesh structure of serpentinites, or the influence of microcracks and pores seems to have a significant influence to the thermal transport properties. We thus conclude that the microstructure dominates the pressure dependence of serpentinites.

4.4. Conductive heat transfer of serpentinites

If we combine the temperature dependence of conductive heat transfer and its pressure derivative, the average intrinsic thermal conductivity of serpentinites can be described as a function of pressure and temperature

$$\lambda = \frac{1}{0.3638 + 0.000244\,T}(1 + 0.148\,P). \qquad (5)$$

T in K, P in GPa, and resultant λ in W/m K.

The experiments show that advective or convective heat transfer may play an important role even at higher temperatures and for very low fluid fractions, which can be responsible for more than 30% of the overall heat transfer. For thermal modelling, especially in a fluid rich environment like subduction zones, advective heat transfer should not be neglected.

Acknowledgements

Thank you H. Kern for your enthusiasm in developing the field of rock physics, for opening the door for colleagues from the former East, and for your support of young scientists, a huge benefit for all of us.

We express our gratitude to A. Ebert and C. Karger for their assistance in thermal conductivity and thermal diffusivity measurements. We want to thank our colleagues D. Bruhn (density), J. Kopp (REM), G. Schäfer (TG/DTA), A. Ullner (TG/DTA), R. Wirth (TEM), and B. Wunder (XRD) for stimulating discussions and essential support. Helpful and constructive reviews by M. Casey, Y.S. Xu, and Editor L. Burlini are gratefully acknowledged. The financial support by the DFG (German science foundation) is gratefully acknowledged.

References

Arndt, J., Bartel, T., Scheuber, E., Schilling, F., 1997. Thermal and elastic properties of crustal rocks from the central Andes. Tectonophysics 271, 75–88.

Balashov, V.N., Yardley, B.W.D., 1998. Modeling metamorphic fluid flow with reaction-compaction-permeability feedbacks. Am. J. Sci. 298, 441–470.

Berman, R., 1984. Thermal Conductivity in Solids. Clareton Univ. Press, Oxford.

Buntebarth, G., 1976. Geothermics. Springer Verlag, Berlin, p. 10ff.

Clauser, Ch., Huenges, E., 1995. Thermal conductivity of rocks and minerals, in rock physics and phase relations. In: Ahrens, Th.J. (Ed.), A Handbook of Physical Constants. American Geophysical Union, AGU Books Board, Washington, DC, pp. 105–126.

Davies, J.H., 1999. The role of hydraulic fractures and intermediate-depth earthquakes in generating subduction-zone magmatism. Nature 398, 142–145.

Eucken, A., 1911. Ueber die Temperaturabhängigkeit der Waermeleitfaehigkeit fester Nichtmetalle. Ann. Phys. (Leipz.) 34, 186–221.

Faust, G.T., Fahey, I.J., 1962. U.S. Geol. Surv. Prof. Pap. 384A, 1–92.

Giese, P., Scheuber, E., Schilling, F.R., Schmitz, M., Wigger, P., 1999. Crustal thickening processes in the central Andes and the different natures of the Moho-discontinuity. J. South Am. Earth Sci. 12, 201–220.

Hoefer, M., Schilling, F.R., 2002. Heat-transfer in quartz, orthoclase, and sanidine at elevated temperature. Phys. Chem. Miner. 29, 571–584.

Kern, H., Liu, B., Popp, T., 1997. Relationship between anisotropy of P and S wave velocities and anisotropy of attenuation in serpentinite and amphibolite. J. Geophys. Res. 102, 3051–3065.

Kirby, S., Engdahl, E.R., Denlinger, R., 1996. Intermediate-depth intraslab earthquakes and arc volcanism as physical expressions of crustal and uppermost mantle metamorphism in subducting slabs. In: Bebout, G.E., Scholl, D.W., Kirby, S.H., Platt, J.P. (Eds.), Subduction Top to Bottom. Geophys. Monogr., vol. 96. Amer. Geophys. Union, Washington, DC, pp. 195–214.

Kittel, Ch., 1983. Introduction to Solid State Physics, 7th ed. Wiley, p. 766.

Kopp, J., 1986, Mineralogical and petrological investigations on serpentinites of the Saxonian Granulite Massif (in German). Thesis, Humboldt-University Berlin.

Pawley, A.R., 1998. The reaction talc + forsterite = enstatite + H_2O: new experimental results and petrological implications. Am. Mineral. 83, 51–57.

Peacock, S.M., 1993. Large-scale hydration above subducting slabs. Chem. Geol. 108, 49–59.

Peacock, S.M., 2001. Are the lower planes of double seismic zones caused by serpentine dehydration in subducting oceanic mantle? Geology 29, 299–302.

Petrunin, G.I., Popov, V.G., 1981. The influence of serpentinization on the thermal properties of ultrabasites (Russian). Fiz. Zemli 4, 18–24.

Petrunin, G.I., Popov, V.G., 1994. Pecularities of the temperature dependence of lattice thermal conductivity of mineralic materials of the earth (Russian). Fiz. Zemli 7, 35–41.

Schilling, F.R., 1997. The effect of fluids on thermal diffusivity of some magmatic rocks. Phys. Chem. Earth 22, 87–91.

Schilling, F.R., 1998. Petrophysik-ein mineralogischer Ansatz, Habilitationsschrift. 259 pp.

Schilling, F.R., 1999. A transient technique to measure thermal diffusivity at elevated temperatures. Eur. J. Mineral. 11, 1115–1124.

Schilling, F.R., Giese, P., Asch, G., Brasse, H., Haberland, Ch., Rietbrock, A., 2000. Fluid/Rock Interaction in the Central Andean Subduction Zone Imaged by Geophysical Observations, extended Abstract. LAK Meeting Stuttgart 2000.

Seipold, U., 1988. Simultaneous measurements of thermal diffusivity and conductivity under high pressure by thermal pulses of finite length. High Temp. High Press. 20, 609–613.

Seipold, U., 1990. Pressure and temperature dependence of thermal transport properties for granites. High Temp. High Press. 22, 541–548.

Seipold, U., 1992. Depth dependence of thermal transport properties for typical crustal rocks. Phys. Earth Planet Inter., 299–303.

Seipold, U., 1995. The variation of the thermal transport properties in the earth's crust. J. Geodyn. 20, 145–154.

Seipold, U., 1996. Measurement of thermal conductivity and thermal diffusivity of serpentinites at high pressure up to 500 MPa. High Temp. High Press. 28, 147–155.

Seipold, U., 1998. Temperature dependence of thermal transport properties of crystalline rocks—a general law. Tectonophysics 291 (1–4), 161–171.

Seipold, U., 2001. Der Wärmetransport in kristallinen Getseinen unter Bedingungen der kontinentalen Kruste. Scientific Technical Report STR01/13. GFZ-Potsdam. 142 pp.

Seipold, U., 2002. Investigation of the thermal transport properties of amphibolites: I. Pressure dependence. High Temp. High Press. 34, 299–306.

Seipold, U., Huenges, E., 1998. Thermal properties of gneisses and amphibolites—high pressure and high temperature investigations of KTB-rock samples. Tectonophysics 291 (1–4), 173–178.

Seipold, U., Mueller, H.J., Tuisku, P., 1998. Principle differences in the high pressure behaviour between thermal and elastic properties of rocks. Phys. Chem. Earth 23 (3), 357–360.

Shannon, R.D., 1976. Revised effective ionic radii and systematic studies of interatomic distances in halides and chalcogenides. Acta Crystallogr., A 32, 751–767.

Slack, G.A., 1973. The thermal conductivity of nonmetallic crystals. Solid State Phys. 34, 1–70.

Springer, M., 1999. Interpretation of heat flow density in the Central Andes. Tectonophysics 306, 377–395.

Tommasi, A., Gibert, B., Seipold, U., Mainprice, D., 2001. Anisotropy of thermal diffusivity in the upper mantle. Nature 411, 783–786.

Ulmer, P., Trommsdorff, V., 1995. Serpentine stability to mantle depth and subduction related magmatism. Science 268, 858–861.

Werner, C.D., 1987. Saxonian granulites-igneous or lithogenous. A contribution to the geochemical diagnosis of the original rocks in high-metamorphic complexes. ZFS-Mitteilungen 133, 221–250.

Wunder, B., Schreyer, W., 1997. Antigorite: high-pressure stability in the system MgO–SiO_2–H_2O (MSH). Lithos 41, 213–227.

Wunder, B., Wirth, R., Gottschalk, M., 2001. Antigorite: pressure and temperature dependence of polysomatism and water content. Eur. J. Miner. 13, 485–495.